Vietnam Journal of Science and Technology ***60*** *(5) (2022) 853-868*

doi:10.15625/2525-2518/16300

DYNAMIC RESPONSE OF FG-CNTRC BEAMS SUBJECTED TO A MOVING MASS

Ismail Esen[1], Thi Thom Tran[2, 3, *], Dinh Kien Nguyen[2, 3]

[1]*Department of Mechanical Engineering, Karabuk University, Makina Mühendisliği Bölümü, Karabük, Turkey*

[2]*Institute of Mechanics, Vietnam Academy of Science and Technology, 18 Hoang Quoc Viet Street, Cau Giay District, Ha Noi, Viet Nam*

[3]*Graduate University of Science and Technology, Vietnam Academy of Science and Technology, 18 Hoang Quoc Viet Street, Cau Giay District, Ha Noi, Viet Nam*

[*]Email: *ttthom@imech.vast.vn*

Received: 18 July 2021; Accepted for publication: 1 September 2021

Abstract. This article presents the forced vibration of composite beams reinforced by single-walled carbon nanotubes (SWCNTs) and subjected to a moving mass. Considering the distribution of carbon nanotubes such as uniform (UD-CNT), functionally graded Λ (FGΛ-CNT) and X (FGX-CNT), three different beams are studied. Based on a third-order shear deformation theory (TSDT), the motion equations of the beams are derived using Hamilton's principle. Including mass interaction forces, the motion equations are transformed into a finite element equation in which a two-node beam element with eight degrees of freedom is utilized. To improve the efficiency of the beam element, the transverse shear rotation is employed as an independent variable in the derivation of the beam element. The vibration characteristics, including the dynamic magnification factors and the time histories for mid-span deflections are computed by using the Newmark method. Numerical result reveal that the vibration of the beams is clearly influenced of the CNT reinforcement, and the dynamic magnification is significantly decreased by increasing the CNT volume fraction. It is also shown that the FGX-CNT beam is the best in dynamic resistance in terms of the lowest dynamic deflection and dynamic magnification factors. The effects of the total volume fraction and the moving load velocity on the dynamic behaviour of the functionally graded carbon nanotube reinforced composites (FG-CNTRC) beams are examined in detail and highlighted.

Keywords: FG-CNTRC beams, third-order shear deformation theory, finite element, moving mass.

Classification numbers: 2.9.4, 5.4.2, 5.4.5.

1. INTRODUCTION

After facing some failure problems caused by delamination and unavoidable micro defects in classical laminated composites, some advanced composites such as carbon nanotubes reinforced composites (CNTRC) have been the subject of extensive researches due to their preferable advantages in the electrical, thermal and mechanical properties. Using molecular dynamics simulations, Bohlén and Bolton [1] reported that the Young's modulus of the composite beams is increased by the oriented CNTs in the used direction. The general rule of mixture for the single-walled carbon nanotubes (SWCNTs) is found to be inaccurate in [2] and then, an extended rule of mixture is proposed in [3]. Some researchers [4, 5] validated the previous results of the mechanical properties of the SWCNT using the finite element method.

Based on the idea of optimal distribution of CNTs, Shen [6] applied the concept of functionally graded material (FGM) to CNTRC and then, the concept of functionally graded carbon nanotube-reinforced composites (FG-CNTRCs) is strongly supported by recent publications. Ke *et al*. [7, 8] used Timoshenko theory to investigate the nonlinear free vibration and dynamic stability of FG nanocomposite beams reinforced with SWCNTs. Also using Timoshenko theory, Yas and Samadi [9] studied free and forced vibration of an FG nanocomposite beam randomly reinforced with straight SWCNTs under a moving load. Free vibration of FG-CNT composite beams was investigated by Lin and Xiang [10] using the first-order shear deformation theory (FSDT) and the third-order shear deformation theory (TSDT). Ansari *et al*. [11] studied the nonlinear forced vibration of FG-CNT Timoshenko beams with the aid of the general differential quadrature method. In [12], using different TSDTs, Aydogdu obtained the natural frequencies of SWCNTRC beams. The nonlinear vibration of imperfect shear deformable FG-CNTRC beams is dealt with by Wu *et al*. [13] based on the FSDT and von Kármán geometric nonlinearity. Chaudhari and Lal [14] investigated the nonlinear free vibration of elastically supported FG-CNT beams in thermal environment. Thermal post-buckling performance of temperature-dependent FG-CNTRC beams with various geometric imperfections was studied by Wu *et al*. [15] based on the FSDT. Gholami *et al*. [16] presented the nonlinear resonant dynamics of geometrically imperfect FG-CNT composite beams subjected to harmonic transverse loads by using the TSDT. Shafiei and Setoodeh [17] investigated nonlinear free vibration and post-buckling of FG-CNT beams on nonlinear foundation. Vo-Duy *et al*. [18] investigated the free vibration behaviour of laminated FG-CNTRC beams using finite element method. Ranjbar *et al*. [19] studied the temperature-dependent of axially FG-CNT reinforced micro-cantilever beams under low velocity impact. For the nonlinear dynamic analysis of FG-CNT beams, Fallah *et al*. [20] proposed a semi-exact solution method. Using a multiscale finite element analysis, Palacios and Ganesan [21] investigated the dynamic response of CNT reinforced-polymer materials.

The problem of moving load maintains its importance in many areas from micro electromechanical systems to bigger space applications. Considering potential advanced applications of the moving load, the dynamics of reinforced composite beams in different types: uniform, X type and Λ type are first modeled using the TSDT and the finite element method in this study. Including the interaction forces of the mass with the beam, the governing equations of the motion of the FG-CNTRC beams are converted to a dynamic finite element equation. A two-node beam element has been developed for the analysis of the whole beam system. The effects of the distribution of CNTs along the beam thickness, the total CNT volume fraction V_{TCNT} and the velocity of the moving mass on the dynamic behaviour of the FG-CNTRC beams are studied in detail.

2. FG-CNT BEAM UNDER A MOVING MASS

Figure 1(a) shows a composite beam with length L, width b, thickness h under a moving mass M. Three types of aligned CNT reinforced beams as shown in Figure 1(b) are considered, namely uniformly distributed CNT beams (UD-CNT), functionally graded CNT beams type X (FGX-CNT), and functionally graded CNT beams type Λ (FGΛ-CNT). The orientations of reinforcing CNT are along the length direction, which is the *x*-axis. The distribution of CNTs in FGΛ-CNTRC beams as a function of *z* coordinate is given by [10]

$$\mu(z)=\left(\frac{h-2z}{2h}\right)^k \quad \text{with } -\frac{h}{2}\le z\le \frac{h}{2} \tag{1}$$

The corresponding volume fraction of CNTs is described by

$$V_{CNT}(z)=(k+1)\left(\frac{h-2z}{2h}\right)^k V_{TCNT} \quad \text{with } -\frac{h}{2}\le z\le \frac{h}{2} \tag{2}$$

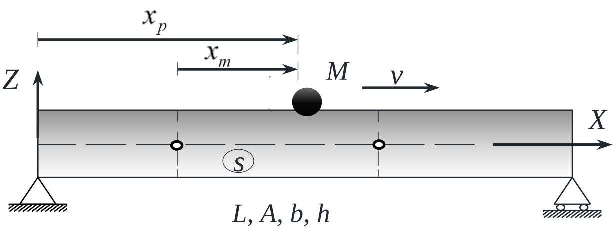

(a)

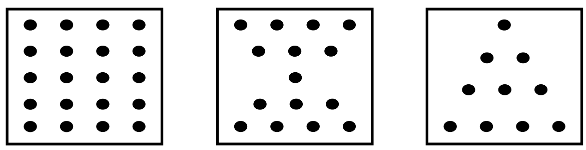

UD-CNT FGX-CNT FGΛ-CNT

(b)

*Figure 1***.** (a) a FG-CNT reinforced beam under a moving mass *M*; (b) cross sections of different beam models, UD-CNT, FGX-CNT and FGΛ-CNT.

However, the manufacturing for such a graded distribution is very costly and difficult. A better way to manufacture CNTRC is to align CNTs functional grading in a polymer matrix and only linear distribution can readily be achieved in engineering practice. So, only linear distribution is considered in the current study, i.e. $k = 1$

$$V_{CNT}(z)=\left(1-\frac{2z}{h}\right)V_{TCNT} \quad \text{with } -\frac{h}{2}\le z\le \frac{h}{2} \tag{3}$$

For FGX-CNT beams, the distribution and volume fraction of CNTs are respectively given by [10]

$$\mu(z)=\begin{cases}\left(\dfrac{2z}{h}\right)^k & \text{with } 0\le z\le \dfrac{h}{2}\\[2ex] \left(-\dfrac{2z}{h}\right)^k & \text{with } -\dfrac{h}{2}\le z\le 0\end{cases} \tag{4}$$

and

$$V_{CNT}(z)=\begin{cases}(k+1)\left(\dfrac{2z}{h}\right)^k V_{TCNT} & \text{with } 0\le z\le \dfrac{h}{2}\\ (k+1)\left(-\dfrac{2z}{h}\right)^k V_{TCNT} & \text{with } -\dfrac{h}{2}\le z\le 0\end{cases} \tag{5}$$

with k = 1,

$$V_{CNT}(z)=\begin{cases}\dfrac{4z}{h}V_{TCNT} & \text{with } 0\le z\le \dfrac{h}{2}\\ -\dfrac{4z}{h}V_{TCNT} & \text{with } -\dfrac{h}{2}\le z\le 0\end{cases} \tag{6}$$

For UD-CNT beams, the CNTs are uniformly dispersed along the thickness of the beam, which makes the CNTs volume fraction along the z coordinate the same as total CNTs volume fraction

$$V_{CNT}(z)=V_{TCNT} \text{ with } -\frac{h}{2}\le z\le \frac{h}{2} \tag{7}$$

The effective material properties are evaluated from the results of MD simulations and mixture rule [2,3]. Hence, the expressions of the properties are [10]

$$\begin{aligned}&E_{11}(z)=\eta_1 V_{CNT}(z)E_{11}^{cnt}+V_m(z)E^m,\\ &E_{22}(z)=\frac{\eta_2}{\dfrac{V_{CNT}(z)}{E_{22}^{cnt}}+\dfrac{V_m(z)}{E^m}},\ G_{12}(z)=\frac{\eta_3}{\dfrac{V_{CNT}(z)}{G_{12}^{cnt}}+\dfrac{V_m(z)}{G^m}},\\ &\upsilon_{21}(z)=\frac{\upsilon_{12}(z)}{E_{11}(z)}E_{22}(z),\ \upsilon_{12}(z)=V_{CNT}(z)\upsilon_{12}^{cnt}+V_m(z)\upsilon^m,\\ &\rho(z)=V_{CNT}(z)\rho^{cnt}+V_m(z)\rho^m,\end{aligned} \tag{8}$$

in which

$$V_m(z)=1-V_{CNT}(z) \tag{9}$$

Here, $E^m, G^m, E_{11}^{cnt}, E_{22}^{cnt}$, and G_{12}^{cnt} are Young’s modulus and shear modulus of matrix and CNT, respectively, $\eta_i\ (i=1,2,3)$ are efficiency parameters of CNT/matrix; υ^m and υ_{12}^{cnt} are Poisson’s ratios of matrix and CNT, and ρ^m and ρ^{cnt} are mass densities of matrix and CNT, respectively.

The effective elastic and shear moduli are calculated as follows [10]

$$E(z)=\frac{E_{11}(z)}{1-\upsilon_{12}(z)\upsilon_{21}(z)},\ G(z)=G_{12}(z) \tag{10}$$

3. GOVERNING EQUATIONS

The Shi's third-order shear deformation theory [22] derived from an elasticity formulation, rather than by the hypothesis of displacements is employed herewith to establish governing equations of the FG-CNTRC beam. This theory, as demonstrated in [22], gives better results than the first-order and other higher order shear deformation theories do. The axial and transverse displacements at any point of the beam are of the form:

$$u(x,z,t)=u_0(x,t)+\frac{z}{4}(5\phi+w_{0,x})-\frac{5z^3}{3h^2}(\phi+w_{0,x}),\ w(x,z,t)=w_0(x,t) \tag{11}$$

In the mid-plane, $u_0(x,t), w_0(x,t)$ are the axial, transverse displacements; ϕ is rotation of the cross section. The transverse shear rotation is defined by [23].

$$\gamma_0=\phi+w_{0,x} \tag{12}$$

Based on Eq. (12), Eq. (11) is modified as

$$u(x,z,t)=u_0(x,t)+z\left(\frac{5}{4}\gamma_0-w_{0,x}\right)-\frac{5z^3}{3h^2}\gamma_0,\ w(x,z,t)=w_0(x,t) \tag{13}$$

The strains related to the displacement field are

$$\varepsilon_{xx}=u_{0,x}+z\left(\frac{5}{4}\gamma_{0,x}-w_{0,xx}\right)-\frac{5z^3}{3h^2}\gamma_{0,x},\ \gamma_{xz}=\left(\frac{5}{4}-\frac{5z^2}{h^2}\right)\gamma_0 \tag{14}$$

The constitutive equation based on Hooke's law is

$$\begin{Bmatrix}\sigma_{xx}\\ \tau_{xz}\end{Bmatrix}=\begin{bmatrix}E(z) & 0\\ 0 & G(z)\end{bmatrix}\begin{Bmatrix}\varepsilon_{xx}\\ \gamma_{xz}\end{Bmatrix} \tag{15}$$

where σ_{xx} and τ_{xz} are the normal and shear stresses, respectively.
From Eqs. (14) and (15), the strain energy (U) of the beam is

$$\begin{aligned}U&=\frac{1}{2}\int_0^L\int_A(\sigma_{xx}\varepsilon_{xx}+\tau_{xz}\gamma_{xz})dAdx\\&=\frac{1}{2}\int_0^L\left[A_{11}u_{0,x}^2+2A_{12}u_{0,x}\left(\frac{5}{4}\gamma_{0,x}-w_{0,xx}\right)+A_{22}\left(\frac{5}{4}\gamma_{0,x}-w_{0,xx}\right)^2-\frac{10}{3h^2}A_{34}u_{0,x}\gamma_{0,x}\right.\\&\left.-\frac{10}{3h^2}A_{44}u_{0,x}\left(\frac{5}{4}\gamma_{0,x}-w_{0,xx}\right)+\frac{25}{9h^4}A_{66}\gamma_{0,x}^2+25\left(\frac{1}{16}B_{11}-\frac{1}{2h^2}B_{22}+\frac{1}{h^4}B_{44}\right)\gamma_0^2\right]dx\end{aligned} \tag{16}$$

where A is the cross-sectional area, and the rigidities $A_{11},A_{12},A_{22},A_{34},A_{44},A_{66}$ and B_{11},B_{22},B_{44} are defined by the following integrations:

$$\begin{aligned}&(A_{11},A_{12},A_{22},A_{34},A_{44},A_{66})=\int_A E(z)(1,z,z^2,z^3,z^4,z^6)dA,\\&(B_{11},B_{22},B_{44})=\int_A G(z)(1,z^2,z^4)dA\end{aligned} \tag{17}$$

For the displacements in Eq. (13), the kinetic energy (T) of the beam is

$$T = \frac{1}{2}\int_0^L \int_A \rho(z)\left(\dot{u}^2 + \dot{w}^2\right) dA dx$$
$$= \frac{1}{2}\int_0^L \left[I_{11}\left(\dot{u}_0^2 + \dot{w}_0^2\right) + 2I_{12}\dot{u}_0\left(\frac{5}{4}\dot{\gamma}_0 - \dot{w}_{0,x}\right) + I_{22}\left(\frac{5}{4}\dot{\gamma}_0 - \dot{w}_{0,x}\right)^2 \right. \tag{18}$$
$$\left. - \frac{10}{3h^2} I_{34}\dot{u}_0\dot{\gamma}_0 - \frac{10}{3h^2} I_{44}\dot{\gamma}_0\left(\frac{5}{4}\dot{\gamma}_0 - \dot{w}_{0,x}\right) + \frac{25}{9h^4} I_{66}\dot{\gamma}_0^2 \right] dx$$

where $\rho(z)$ is the mass density. The symbol (.) represents the time derivative, and the mass moments in Eq. (18) are derived as follows

$$\left(I_{11}, I_{12}, I_{22}, I_{34}, I_{44}, I_{66}\right) = \int_A \rho(z)\left(1, z, z^2, z^3, z^4, z^6\right) dA \tag{19}$$

The kinetic energy T_m of the moving mass is [24]

$$T_m = \frac{1}{2} M \left(v^2 + \left(\dot{w} + v w_{,x}\right)^2_{x = x_p} \right) \tag{20}$$

Due to the interaction with the moving mass, the potential energy of the composite beam is [25].

$$V = M\left[g - \ddot{w}\left(x_p, t\right)\right] w(x,t)\,\delta\left(x - x_p(t)\right) \tag{21}$$

where $\delta(.)$ is the Dirac delta function, g is the acceleration of gravity, $M\ddot{w}\left(x_p, t\right)$ is the interaction force, $x_p(t)$ is the time dependent location of the mass at time t, and given by $x_p(t) = vt$. From the total exact differentiation of $w(x,t)$ with respect to x_p, the interaction force in z direction can be derived as [25]:

$$f_z(x,t) = Mg - M\left(\ddot{w} + 2v\dot{w}_{,x} + v^2 w_{,xx}\right)\delta\left(x - x_p\right) \tag{22}$$

When Eqs. (16), (18), (20) and (21) are used in Hamilton's principle, the following forced equations of the motion can be derived for the composite beam and moving mass system:

$$I_{11}\ddot{u}_0 + I_{12}\left(\frac{5}{4}\ddot{\gamma}_0 - \ddot{w}_{0,x}\right) - I_{34}\frac{5}{3h^2}\ddot{\gamma}_0 - \frac{\partial}{\partial x}\left[A_{11}u_{0,x} + A_{22}\left(\frac{5}{4}\gamma_{0,x} - w_{0,xx}\right) - A_{34}\frac{5}{3h^2}\gamma_{0,x}\right] = 0 \tag{23a}$$

$$I_{11}\ddot{w}_0 + \frac{\partial}{\partial x}\left[I_{12}\ddot{u}_0 + I_{22}\left(\frac{5}{4}\ddot{\gamma}_0 - \ddot{w}_{0,x}\right) - I_{44}\frac{5}{3h^2}\ddot{\gamma}_0 \right]$$
$$- \frac{\partial^2}{\partial x^2}\left[A_{12}u_{0,x} + A_{22}\left(\frac{5}{4}\gamma_{0,x} - w_{0,xx}\right) - A_{44}\frac{5}{3h^2}\gamma_{0,x}\right] \tag{23b}$$
$$+ \left(M\ddot{w}_0 + 2Mv\dot{w}_{0,x} + Mv^2 w_{0,xx} - Mg\right)_{x = x_p} = 0$$

$$\frac{1}{4}I_{12}\ddot{u}_0+\frac{1}{4}I_{22}\left(\frac{5}{4}\ddot{\gamma}_0-\ddot{w}_{0,x}\right)-I_{34}\frac{1}{3h^2}\ddot{u}_0-I_{44}\frac{1}{3h^2}\left(\frac{5}{2}\ddot{\gamma}_0-\ddot{w}_{0,x}\right)+I_{66}\frac{5}{9h^4}\ddot{\gamma}_0$$
$$-\frac{\partial}{\partial x}\left[\frac{1}{4}A_{12}u_{0,x}+\frac{1}{4}A_{22}\left(\frac{5}{4}\gamma_{0,x}-w_{0,xx}\right)-A_{34}\frac{1}{3h^2}u_{0,x}-A_{44}\frac{1}{3h^2}\left(\frac{5}{2}\gamma_{0,x}-w_{0,xx}\right)-A_{66}\frac{5}{9h^4}\gamma_{0,x}\right] \quad (23c)$$
$$+5\left(\frac{1}{16}B_{11}-\frac{1}{2h^2}B_{22}+\frac{1}{h^4}B_{44}\right)\gamma_0=0$$

4. FINITE ELEMENT MODELLING

4.1. Element formulation

Including the mass interaction terms, the derivation of the closed form solution of the system of differential equations (23) is difficult. But by using proper nodal variables, a finite element formulation can be easily achieved using a two-node beam element. In this study, the beam is divided into two-node beam elements with length l and each node has four nodal variables with axial and transverse displacements u_0 and w_0, derivation of transverse displacement $w_{0,x}$, and transverse shear rotation γ_0. Considering these variables, the vector of the displacements of proposed beam element is of the form:

$$\mathbf{d}=\begin{bmatrix}u_{01} & w_{01} & w_{0,x1} & \gamma_{01} & u_{02} & w_{02} & w_{0,x2} & \gamma_{0,2}\end{bmatrix}^T \quad (24)$$

The displacements inside the beam element can be calculated from the nodal values using proper interpolation functions, where,

$$u_0=\mathbf{N}_{\boldsymbol{u}}\mathbf{d},\ \gamma_0=\mathbf{N}_\gamma\mathbf{d},\ w_0=\mathbf{N}_w\mathbf{d} \quad (25)$$

Here, linear interpolation functions are used for $\mathbf{N}_u$, $\mathbf{N}_\gamma$, Hermite interpolation functions are adopted for $\mathbf{N}_w$. They are considered as given below:

$$\begin{aligned}\mathbf{N}_u&=\begin{bmatrix}N_{u1} & N_{u2} & N_{u3} & N_{u4} & N_{u5} & N_{u6} & N_{u7} & N_{u8}\end{bmatrix}\\ \mathbf{N}_\gamma&=\begin{bmatrix}N_{\gamma1} & N_{\gamma2} & N_{\gamma3} & N_{\gamma4} & N_{\gamma5} & N_{\gamma6} & N_{\gamma7} & N_{\gamma8}\end{bmatrix}\\ \mathbf{N}_w&=\begin{bmatrix}N_{w1} & N_{w2} & N_{w3} & N_{w4} & N_{w5} & N_{w6} & N_{w7} & N_{w8}\end{bmatrix}\end{aligned} \quad (26)$$

with

$$\begin{aligned}&N_{u1}=1-\frac{x}{l},\ N_{u5}=\frac{x}{l}, N_{u2}=N_{u3}=N_{u4}=N_{u6}=N_{u7}=N_{u8}=0\\ &N_{\gamma4}=1-\frac{x}{l},\ N_{\gamma8}=\frac{x}{l},\ N_{\gamma1}=N_{\gamma2}=N_{\gamma3}=N_{\gamma5}=N_{u\gamma6}=N_{u\gamma7}=0\\ &N_{w2}=1-3\left(\frac{x}{l}\right)^2+2\left(\frac{x}{l}\right)^3,\ N_{w3}=x-2\frac{x^2}{l}+\frac{x^3}{l^2}, N_{w6}=3\left(\frac{x}{l}\right)^2-2\left(\frac{x}{l}\right)^3,\ N_{w7}=-\frac{x^2}{l}+\frac{x^3}{l^2}\\ &N_{w1}=N_{w4}=N_{w5}=N_{w8}=0\end{aligned} \quad (27)$$

Including the potential energy from the interaction terms in Eq. (21) and using Eq. (16), the total strain energy of the beam having *r* finite elements can be written as

$$U = \frac{1}{2}\sum_{i}^{r} \mathbf{d}^{\mathrm{T}}\mathbf{k}\mathbf{d} \tag{28}$$

where the element stiffness matrix **k** is in the form

$$\mathbf{k} = \mathbf{k}_{uu}^{11} + \mathbf{k}_{u\gamma}^{12} + \mathbf{k}_{\gamma\gamma}^{22} + \mathbf{k}_{u\gamma}^{34} + \mathbf{k}_{\gamma\gamma}^{44} + \mathbf{k}_{\gamma\gamma}^{66} + \mathbf{k}_{ss} + \mathbf{k}_{m}\big|_{i=s} \tag{29}$$

with

$$\begin{aligned}
&\mathbf{k}_{uu}^{11} = \int_0^l \mathbf{N}_{u,x}^T A_{11} \mathbf{N}_{u,x} dx,\ \mathbf{k}_{u\gamma}^{12} = \int_0^l \mathbf{N}_{u,x}^T A_{12} \left(\frac{5}{4}\mathbf{N}_{\gamma,x} - \mathbf{N}_{w,xx}\right) dx,\\
&\mathbf{k}_{\gamma\gamma}^{22} = \int_0^l \left(\frac{5}{4}\mathbf{N}_{\gamma,x}^T - \mathbf{N}_{w,xx}^T\right) A_{22} \left(\frac{5}{4}\mathbf{N}_{\gamma,x} - \mathbf{N}_{w,xx}\right) dx,\ \mathbf{k}_{u\gamma}^{34} = -\frac{5}{3h^2}\int_0^l \mathbf{N}_{u,x}^T A_{34} \mathbf{N}_{\gamma,x} dx,\\
&\mathbf{k}_{\gamma\gamma}^{44} = -\int_0^l \left(\frac{5}{4}\mathbf{N}_{\gamma,x}^T - \mathbf{N}_{w,xx}^T\right) A_{44} \mathbf{N}_{\gamma,x},\ \mathbf{k}_{\gamma\gamma}^{66} = \frac{25}{9h^4}\int_0^l \mathbf{N}_{\gamma,x}^T A_{66} \mathbf{N}_{\gamma,x} dx,\\
&\mathbf{k}_{ss} = 25\int_0^l \mathbf{N}_{\gamma}^T \left(\frac{1}{16}B_{11} - \frac{1}{2h^2}B_{22} + \frac{1}{h^4}B_{44}\right) \mathbf{N}_{\gamma} dx,\ \mathbf{k}_{m}\big|_{i=s} = \mathbf{N}_{w,xx}^T M v^2 \mathbf{N}_w
\end{aligned} \tag{30}$$

Considering Eqs. (18) and (20), the total kinetic energy is

$$T = \frac{1}{2}\sum_{i}^{r} \dot{\mathbf{d}}^{\mathbf{T}}\mathbf{m}\dot{\mathbf{d}} \tag{31}$$

where the element mass matrix **m** is in the form

$$\boldsymbol{m} = \mathbf{m}_{uu}^{11} + \mathbf{m}_{ww}^{11} + \mathbf{m}_{u\gamma}^{12} + \mathbf{m}_{\gamma\gamma}^{22} + \mathbf{m}_{u\gamma}^{34} + \mathbf{m}_{\gamma\gamma}^{44} + \mathbf{m}_{\gamma\gamma}^{66} + \mathbf{m}_{m}\big|_{i=s} \tag{32}$$

with

$$\begin{aligned}
&\mathbf{m}_{uu}^{11} = \int_0^l \mathbf{N}_u^T I_{11} \mathbf{N}_u dx,\ \ \mathbf{m}_{ww}^{11} = \int_0^l \mathbf{N}_w^T I_{11} \mathbf{N}_w dx,\ \mathbf{m}_{u\gamma}^{12} = \int_0^l \mathbf{N}_u^T I_{12} \left(\frac{5}{4}\mathbf{N}_{\gamma} - \mathbf{N}_{w,x}\right) dx,\\
&\mathbf{m}_{\gamma\gamma}^{22} = \int_0^l \left(\frac{5}{4}\mathbf{N}_{\gamma}^T - \mathbf{N}_{w,x}^T\right) I_{22} \left(\frac{5}{4}\mathbf{N}_{\gamma} - \mathbf{N}_{w,x}\right) dx,\ \mathbf{m}_{u\gamma}^{34} = -\frac{5}{3h^2}\int_0^l \mathbf{N}_u^T I_{34} \left(\mathbf{N}_{\gamma} - \mathbf{N}_{w,x}\right) dx,\\
&\mathbf{m}_{\gamma\gamma}^{44} = -\int_0^l \left(\frac{5}{4}\mathbf{N}_{\gamma,x}^T - \mathbf{N}_{w,xx}^T\right) I_{44} \mathbf{N}_{\gamma,x},\ \ \mathbf{m}_{\gamma\gamma}^{66} = \frac{25}{9h^4}\int_0^l \mathbf{N}_{\gamma}^T I_{66} \mathbf{N}_{\gamma} dx,\ \mathbf{m}_{m}\big|_{i=s} = \mathbf{N}_w^T M \mathbf{N}_w
\end{aligned} \tag{33}$$

4.2. Modelling of the damping

The viscous damping matrix of the FG-CNTRC beam element can be determined through the Rayleigh damping as

$$\mathbf{c} = a_0\mathbf{m} + a_1\mathbf{k},\ a_0 = \frac{2\omega_i\omega_j\left(\xi_i\omega_j - \xi_j\omega_i\right)}{\omega_j^2 - \omega_i^2}, a_1 = \frac{2\left(\xi_j\omega_j - \xi_i\omega_i\right)}{\omega_j^2 - \omega_i^2} \tag{34}$$

where $\mathbf{m}$ and $\mathbf{k}$ are the property matrices of the beam element, ξ_i and ξ_j are damping ratios related to natural frequencies ω_i and ω_j. In this paper, the damping ratios $\xi_1 = \xi_2 = 0.005$ are used. The Coriolis force component $2Mv\dot{w}_{,x}$ in (22) can be derived for the contacted beam element s as given below:

$$\mathbf{c}_m\big|_{i=s} = 2vM\mathbf{N}_{w,x}^T\mathbf{N}_w \tag{35}$$

4.3. Equation of motion of the entire system

The motion equation of the whole system shown in Figure 1 is

$$\mathbf{M}\ddot{\mathbf{q}} + \mathbf{C}\dot{\mathbf{q}} + \mathbf{K}\mathbf{q} = \mathbf{F} \tag{36}$$

where, **M**, **C**, and **K** are the global mass, damping and stiffness matrices, respectively; $\ddot{\mathbf{q}}$, $\dot{\mathbf{q}}$ and $\mathbf{q}$ are the vectors of acceleration, velocity, and displacement, respectively; and **F** is the nodal external force at time *t*. The global stiffness, mass and damping matrices are obtained using the property matrices in (30), (33) and (34), respectively. The matrices $\mathbf{k}_m\big|_{i=s}$ and $\mathbf{m}_m\big|_{i=s}$ and $\mathbf{c}_m\big|_{i=s}$ in (30), (33) and (35) resulting from mass interaction are only added to the matrices of the element *s*. The nodal external force **F** is constituted of zeros, except for the coefficients of the instantaneous element nodal force vector $\mathbf{f}$ of the element *s* as

$$\mathbf{F} = \begin{bmatrix} 0 & \ldots & \mathbf{f} & \ldots & 0 \end{bmatrix}^{\mathrm{T}} \tag{37}$$

with

$$\mathbf{f} = Mg\mathbf{N}_w^T \tag{38}$$

Newmark method is used herein to solve the equation of motion (36) for obtaining the beam deflections.

5. RESULTS AND DISCUSSION

5.1. Validation

Table 1. Comparison of frequency parameter of FG-CNTRC with *L/h* = 12.

Distribution	Source	$V_{TCNT} = 0.12$	$V_{TCNT} = 0.17$	$V_{TCNT} = 0.28$
UD-CNT	Lin and Xiang [10]	12.4402	15.2313	17.2125
	Present	12.4401	15.2314	17.2125
FGΛ-CNT	Lin and Xiang [10]	12.1604	14.8671	16.9276
	Present	12.1618	14.8689	16.9308
FGX-CNT	Lin and Xiang [10]	13.7748	16.9068	18.5193
	Present	13.7748	16.9068	18.5208

Table 1 shows the comparison of the fundamental frequency parameter for different total CNT volume fractions V_{TCNT}. The fundamental frequency parameter is defined in [10] and slenderness ratio is $L/h = 12$. Very good agreement between the frequency parameter of the present work and that of [10], regardless of the total CNT volume fraction V_{TCNT} and CNT distribution, is seen from Table 1, noting that Lin and Xiang computed the fundamental frequency parameter in Table 1 based on the TSDT and the Ritz method.

5.2. Case study

Noting that the input data in [10] is used to receive the results in Table 1 and to compute the below results. The thickness and width of the beams are $h = b = 1$ m. A moving mass $M = 100\,\text{kg}$ is employed in all computations. The number of the finite elements is set to 20, and a uniform increment time step $\Delta t = \Delta T/200$ where ΔT is the total time necessary for the mass crossing the beam, is used for the Newmark procedure. For the convenience of discussion, the following dynamic magnification factor D_d is introduced.

$$D_d = \max\left(\frac{w(L/2,t)}{w_{st}}\right), \tag{39}$$

where $w_{st} = L^3 Mg/48E_m I$ is the static deflection of a fully matrix material beam under the load $F = Mg$ acting at the mid-span.

Table 2. Dynamic magnification factors for three different types of FG distribution.

L/h	Distribution	$V_{TCNT}=0.12$			$V_{TCNT}=0.17$			$V_{TCNT}=0.28$		
		$v=20$ (m/s)	$v=80$ (m/s)	$v=150$ (m/s)	$v=20$ (m/s)	$v=80$ (m/s)	$v=150$ (m/s)	$v=20$ (m/s)	$v=80$ (m/s)	$v=150$ (m/s)
5	UD-CNT	0.1596	0.1686	0.1753	0.0975	0.1038	0.1023	0.0794	0.0849	0.0867
	FGΛ-CNT	0.1623	0.1719	0.1792	0.0994	0.1053	0.1032	0.0793	0.0848	0.0866
	FGX-CNT	0.1458	0.1518	0.1554	0.0901	0.0970	0.0974	0.0772	0.0824	0.0847
10	UD-CNT	0.0631	0.0706	0.0825	0.0400	0.0425	0.0438	0.0302	0.0299	0.0301
	FGΛ-CNT	0.0656	0.0733	0.0875	0.0420	0.0450	0.0468	0.0311	0.0311	0.0314
	FGX-CNT	0.0536	0.0595	0.0656	0.0338	0.0340	0.0344	0.0270	0.0276	0.0261
20	UD-CNT	0.0363	0.0411	0.0564	0.0242	0.0243	0.0359	0.0164	0.0180	0.0225
	FGΛ-CNT	0.0397	0.0455	0.0615	0.0265	0.0260	0.0393	0.0177	0.0190	0.0245
	FGX-CNT	0.0279	0.0272	0.0411	0.0182	0.0198	0.0249	0.0129	0.0144	0.0160
30	UD-CNT	0.0323	0.0445	0.0509	0.0217	0.0270	0.0342	0.0137	0.0153	0.0213
	FGΛ-CNT	0.0357	0.0496	0.0552	0.0237	0.0304	0.0376	0.0150	0.0171	0.0235
	FGX-CNT	0.0230	0.0286	0.0357	0.0150	0.0168	0.0235	0.0100	0.0101	0.0148

Table 2 lists the dynamic magnification factors for three different types of the CNT distribution at different values of the mass velocity. Four values of aspect ratio *L/h* are chosen to compute the factor D_d. It is seen from the table that the factor D_d decreases with increasing the total CNT volume fraction V_{TCNT}, regardless of the aspect ratio and the mass velocity. Of the three types of the CNT distribution, the factor D_d received from FGX-CNT beam is the smallest. The results obtained for the beam with UD and FGΛ distributions are quite close together, especially at higher values of the aspect ratio *L/h*. Table 2 also shows the effect of the aspect ratio *L/h* on the dynamic behaviour of the beam, the factor D_d decreases sharply by increasing *L/h*. Furthermore, as in the case of the isotropic beams, the dynamic magnification factor D_d tends to increase as the moving load velocity increases. The dependence of the factor D_d on the total CNTs volume fraction and the velocity of the moving mass for three types of the CNT distribution will be observed more clearly through the figures below for the beam with an aspect ratio $L/h = 20$.

Figure 2 shows the dynamic magnification factors D_d of the UD-CNT, FGΛ-CNT and FGX-CNT beams according to the velocity of the moving mass for three values of the total volume fraction of CNTs, $V_{TCNT} = 0.12$, 0.17 and 0.28. From this figure, the dynamic characteristics of the UD-CNT and FGΛ-CNT beams appear to be quite close, and when compared to each other, the UD-CNT beam is weaker than the FGΛ-CNT beam. Moreover, the maximum values of D_d for the UD-CNT and FGΛ-CNT beams, as listed in Table 3, appear earlier than the FGX-CNT beam.This means that the FGX-CNT beam is better than the others in terms of resonance performance. One of the reasons for this feature of the FGX-CNT beam is that the effective mass is distributed close to the lower and upper planes of the beam, away from the beam mid-plane.

As shown in Figure 2 and listed in Table 3, as the total volume fraction of CNTs increases, the velocity of the moving mass at which the maximum dynamic magnification factors occur in all beam types also increases.

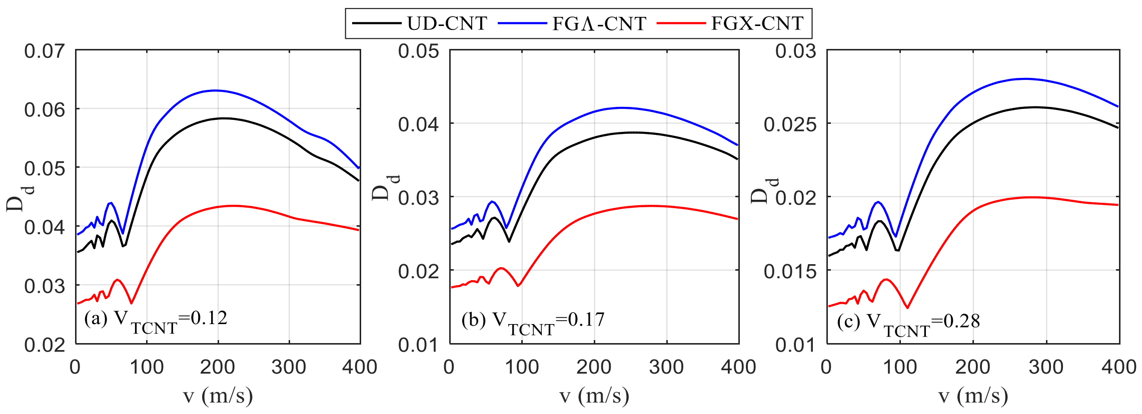

Figure 2. Comparison of dynamic magnification factors for three different FG-CNTRC beams.

Table 3. Maximum dynamic factor D_d and corresponding moving mass velocity for three different beams.

V_{TCNT}	0.12			0.17			0.28		
Beam Type	FGΛ-CNT	UD-CNT	FGX-CNT	FGΛ-CNT	UD-CNT	FGX-CNT	FGΛ-CNT	UD-CNT	FGX-CNT
v (m/s)	195	206	222	234	254	278	274	282	286
Max D_d	0.06303	0.05831	0.04343	0.04207	0.03871	0.02873	0.02801	0.02608	0.01995

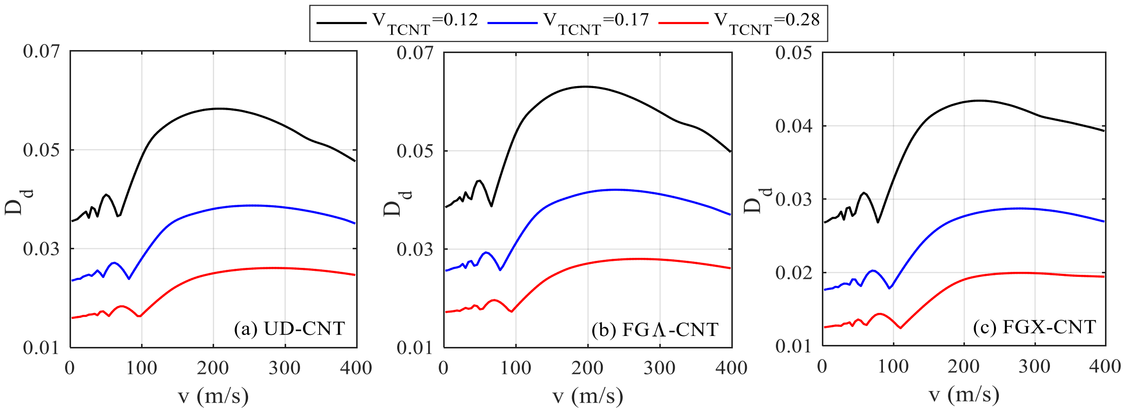

Figure 3. Comparison of dynamic magnification factors for $V_{TCNT}=0.12, 0.17, 0.28$

This means that the CNT addition raises the resonant frequency of the beam and the possible resonance will occur at higher speeds of the moving mass. From this, we can conclude that CNT reinforcement will provide a better dynamic behaviour compared to beams that are not reinforced, and this result may be useful for beams to be used in high-speed applications of the moving mass problems.

Similar to the results of the previous analysis, Figure 3 and Table 4 show that the FGX-CNT beam has the best resonance behaviour, which shows maximum factor D_d at higher speeds of the mass when compared to the other beam types. The UD-CNT beam looks slightly better than the FGΛ-CNT beam in terms of the mass velocity at which it undergoes resonance. The increase in the total volume fraction of CNTs in all three beam types causes maximum factor D_d to occur at higher mass velocities. That is, the addition of CNT improves the dynamic behaviour of the beam, which would be advantageous for applications where high strength, lightness and better resonance behaviour are desired.

Table 4. Maximum dynamic factor D_d and corresponding moving mass velocity for beams with $V_{TCNT}=0.12, 0.17, 0.28$.

Beam Type	UD-CNT			FGΛ-CNT			FGX-CNT		
V_{TCNT}	0.12	0.17	0.28	0.12	0.17	0.28	0.12	0.17	0.28
v (m/s)	210	250	282	198	234	270	222	274	286
Max D_d	0.05830	0.03871	0.02608	0.06303	0.04207	0.02801	0.04343	0.02873	0.01995

To better understand the dynamic behaviour of FG-CNTRC beams, it is necessary to look at the time histories for dimensionless mid-span transverse displacement of the beams under the moving mass. Figure 4 shows the time histories for dimensionless mid-span transverse displacement for the UD-CNT beam with different total CNT volume fractions $V_{TCNT}=0.12, 0.17$ and 0.28. Three values of the velocity of the moving mass, v=20, 50 and 100 m/s, are chosen to plot the figure. It is seen that the mid-span deflection of the UD-CNT beam is different, and it is dependent on the CNT amount. The number of the full vibration waves seen in the response curves can be used to recognise the dynamic characteristics of the beam. Thus, in the curves given comparatively, the beam with the highest number of vibration waves behaves more rigid than the others and this beam is further away from the resonance zone for this speed. As can be observed from the curves in the graphs, for the UD-CNT beam with a higher CNT addition, the number of waves is higher than those with less CNT. As seen from the curves in the figure, the beam with the lowest total CNT volume fraction, $V_{TCNT} = 0.12$, has the highest vibration amplitude and the one with $V_{TCNT} = 0.28$ has the lowest vibration amplitude.

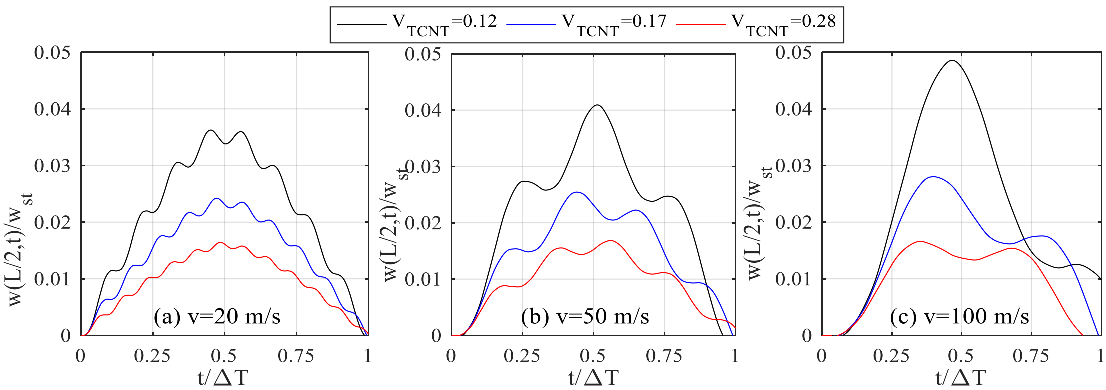

Figure 4. Time histories for dimensionless mid-span transverse displacement of UD-CNTRC beams.

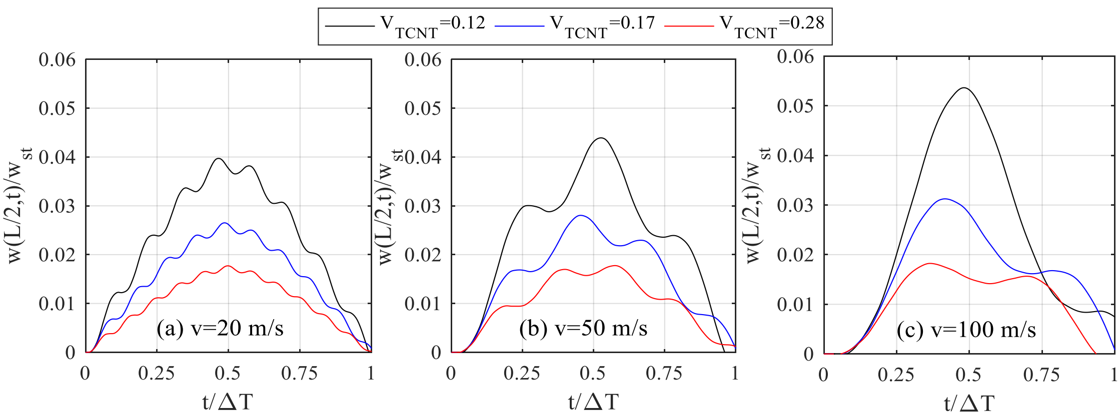

Figure 5. Time histories for dimensionless mid-span transverse displacement of FGΛ -CNTRC beams.

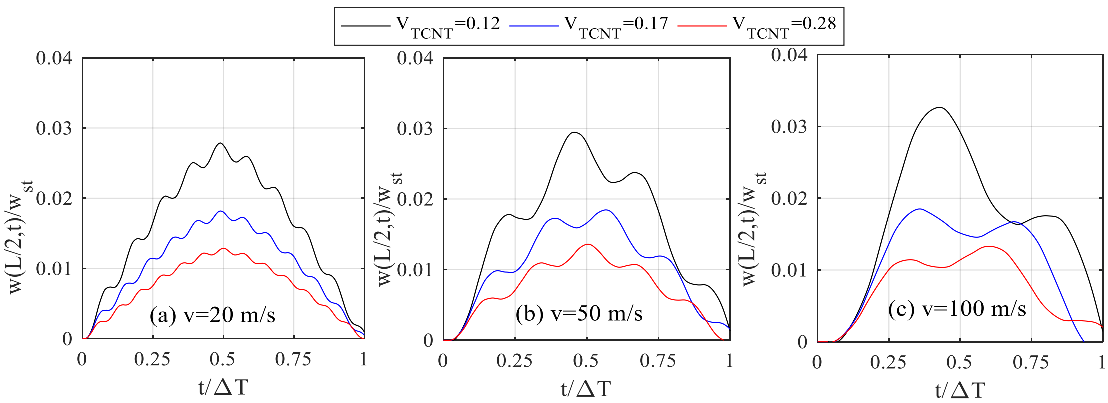

Figure 6. Time histories for dimensionless mid-span transverse displacement of FGX-CNTRC beams.

Similarly, the time histories for dimensionless mid-span transverse displacement of the FGΛ-CNT and FGX-CNT beams are given in Figures 5 and 6, respectively, for the same values of V_{TCNT} and v. It is observed from the figures that the FGX-CNTRC beams create smaller vibration amplitudes for the same load velocities since they are far from the resonance zone. In this respect, in the dynamics of FG-CNTRC beams, the total volume fractions of CNTs and the distribution of CNTs along the thickness are important. Thus, in moving mass applications, it is possible to design a FG-CNTRC beam that can give the best dynamic performance for the mass and speed of the mass.

6. CONCLUSIONS

In this study, the dynamic behaviour of FG-CNTRC beams interacting with a moving mass is modelled and analysed. Using the third-order shear deformation theory in modelling, equations of motion are transformed into a finite element equation. A two-node finite beam element has been developed and the beam domain has been discretised. The developed finite element, which has axial elongation, transverse displacement, spatial derivative of transverse displacement and shear rotation degrees of freedom at the node points, has a total of 8 degrees of freedom. The obtained modelling was compared with the literature study and the finite element number was determined in terms of calculation accuracy. Three types of FG-CNTRC beams, namely UD-CNT, FGΛ-CNT and FGX-CNT beams, are modelled and their dynamic behaviours under the moving mass are analysed. Generally, it is understood from the analysis results that CNT addition improves the dynamic behaviour of beams of all types and this improvement increases with increasing the amount of CNTs. With the addition of CNTs, the FG-CNTRC beams behave stronger and the mass travelling velocity at which maximum displacement occurs increases. This also means that using FG-CNTRC beams for high-speed applications will bring an application advantage.

In addition, the distribution of the CNTs along the beam thickness is also important besides the total volume fractions of CNTs since the dynamic enhancement of the mixture model type X of the FGX-CNT beams, in which CNTs are concentrated on the lower and upper surfaces of the beam, is better than the other types. For the same amount of total volume fractions of CNTs, the dynamic behaviours of the FGΛ-CNT and UD-CNT beams are close to each other. It is understood from the analysis that the stiffness of the beams increases with increasing the amount of CNTs in all beam types. Using the method proposed in this study, it is possible to design and analyze an FG-CNTRC beam that can meet the desired dynamic properties for use in a moving load application.

Authors contributions: Dr. Ismail Esen: set up the problem. Dr. Thi Thom Tran: developed the computer code, prepared the manuscript. Dr. Dinh Kien Nguyen: checked the results and final manuscript.

Declaration of competing interest. We declare that we have no known competing financial interests or personal relationships that could have appeared to influence the work reported in this paper.

REFERENCES

1. Bohlén M. and Bolton K. - Molecular dynamics studies of the influence of single wall carbon nanotubes on the mechanical properties of Poly(vinylidene fluoride), Comput. Mater. Sci. **68** (2013) 73-80.
2. Han Y. and Elliott J. - Molecular dynamics simulations of the elastic properties of polymer/carbon nanotube composites, Comput. Mater. Sci. **39** (2007) 315-323.

3. Griebel M. and Hamaekers J. - Molecular dynamics simulations of the elastic moduli of polymer–carbon nanotube composites, Comput. Methods Appl. Mech. Engrg. **193** (2004) 1773-1788.
4. Lu X. and Hu Z. - Mechanical property evaluation of single-walled carbon nanotubes by finite element modeling, Compos. Part B: Eng. **43** (2012) 1902-1913.
5. Giannopoulos G. I., Kakavas P. A., and Anifantis N. K. - Evaluation of the effective mechanical properties of single walled carbon nanotubes using a spring based finite element approach, Comput.Mater. Sci. **41** (2008) 561-569.
6. Shen H. S. - Nonlinear bending of functionally graded carbon nanotube-reinforced composite plates in thermal environments, Compos. Struct. **91** (2009) 9-19.
7. Ke L. L., Yang J., and Kitipornchai S. - Nonlinear free vibration of functionally graded carbon nanotubereinforced composite beams, Compos. Struct. **92** (2010) 676-683.
8. Ke L. L., Yang J., and Kitipornchai S. - Dynamic stability of functionally graded carbon nanotube- reinforced composite beams, Mech. Adv. Mater. Struct. **20** (2013) 28-37.
9. Yas M. H. and Heshmati M. - Dynamic analysis of functionally graded nanocomposite beams reinforced by randomly oriented carbon nanotube under the action of moving load, Appl. Math. Model. **36** (2012) 1371-94.
10. Lin F. and Xiang Y. - Vibration of carbon nanotube reinforced composite beams based on the first and third order beam theories, Appl. Math. Model. **38** (2014) 3741-3754.
11. Ansari R., Faghih Shojaei M., Mohammadi V., Gholami R., and Sadeghi F. - Nonlinear forced vibration analysis of functionally graded carbon nanotube-reinforced composite Timoshenko beams, Compos. Struct. **13** (2014) 316-327.
12. Aydogdu M. - On the vibration of aligned carbon nanotube reinforced composite beams, Adv. Nano Res. **2** (2014) 199-210.
13. Wu. H. L., Yang J., and Kitipornchai S. - Nonlinear vibration of functionally graded carbon nanotube-reinforced composite beams with geometric imperfections, Compos. Part B: Eng. **90** (2016) 86-96.
14. Chaudhari V. K. and Lal A. - Nonlinear Free Vibration Analysis of Elastically Supported Nanotube-reinforced Composite Beam in Thermal Environment, Proc. Eng. **144** (2016) 928-935.
15. Wu H., Kitipornchai S. and Yang J. - Imperfection sensitivity of thermal post-buckling behaviour of functionally graded carbon nanotube-reinforced composite beams, Appl. Math. Model. **42** (2017) 735-752.
16. Gholami R., Ansari R., and Gholami Y. - Nonlinear resonant dynamics of geometrically imperfect higher-order shear deformable functionally graded carbon-nanotube reinforced composite beams, Compos. Struct. **174** (2017) 45-58.
17. Shafiei H. and Setoodeh A. R. - Nonlinear free vibration and post-buckling of FG-CNTRC beams on nonlinear foundation, Steel. Compos. Struct. **24** (2017) 65-77.
18. Vo-Duy T., Ho-Huu V. and Nguyen-Thoi T. - Free vibration analysis of laminated FG-CNT reinforced composite beams using finite element method, Front. Struct. Civil. Eng. **13** (2019) 324-336.
19. Ranjbar M. and Feli S. - Temperature-dependent analysis of axially functionally graded CNT reinforced micro-cantilever beams subjected to low velocity impact, Mech. Adv. Mater. Struct. **26** (2019) 1154-1168.

20. Fallah A., Dehkordi M. B., Nourbakhsh H., and Beni Y. T. - Semi-exact solution for nonlinear dynamic analysis of graded carbon nanotube-reinforced beam with graded shape memory wires, Mech. Adv. Mater. Struct. **28** (2019) 1-15.
21. Palacios J. A. and Ganesan R. - Dynamic response of Carbon-Nanotube-Reinforced-Polymer materials based on multiscale finite element analysis, Compos. Part B: Eng. **166** (2019) 497-508.
22. Shi G. - A new simple third-order shear deformation theory of plates, Int. J. Solids Struct. **44** (2007) 4399-417.
23. Shi G., Lam K. Y. and Tay T. E. - On efficient finite element modeling of composite beams and plates using higher-order theories and an accurate composite beam element, Compos. Struct. **41** (1998) 159-165.
24. Esen I. -Dynamic response of a functionally graded Timoshenko beam on two-parameter elastic foundations due to a variable velocity moving mass, Int. J. Mech. Sci. **153–154** (2019) 21-35.
25. Esen I. - A new finite element for transverse vibration of rectangular thin plates under a moving mass, Finite Elem. Anal. Des. **66** (2013) 26-35.